ISSN 0006-2979, Biochemistry (Moscow), 2012, Vol. 77, No. 8, pp. 901-909. © Pleiades Publishing, Ltd., 2012.
Published in Russian in Biokhimiya, 2012, Vol. 77, No. 8, pp. 1095-1104.
Originally published in Biochemistry (Moscow) On-Line Papers in Press, as Manuscript BM12-049, June 17, 2012.

Effect of Calcium Ions on Electron Transfer between Hemes *a* and a_3 in Cytochrome *c* Oxidase

T. V. Vygodina*, A. V. Dyuba, and A. A. Konstantinov

Belozersky Institute of Physico-Chemical Biology, Lomonosov Moscow State University, 119991 Moscow, Russia; E-mail: vygodina@genebee.msu.ru

Received February 28, 2012
Revision received March 15, 2012

Abstract—Kinetics of the reduction of the hemes in cytochrome *c* oxidase in the presence of high concentration of ruthenium(III)hexaammine chloride was examined using a stopped-flow spectrophotometer. Upon mixing of the oxidized enzyme with dithionite and $Ru(NH_3)_6^{3+}$, three well-resolved phases were observed: heme *a* reduction reaching completion within a few milliseconds is followed by two slow phases of heme a_3 reduction. The difference spectrum of heme a_3 reduction in the visible region is characterized by a maximum at ~612 nm, rather than at 603 nm as was believed earlier. It is shown that in the case of bovine heart cytochrome *c* oxidase containing a special cation-binding site in which reversible binding of calcium ion occurs, heme a_3 reduction is slowed down by low concentrations of Ca^{2+}. The effect is absent in the case of the bacterial cytochrome oxidase in which the cation-binding site contains a tightly bound Ca^{2+} ion. The data corroborate the inhibition of the cytochrome oxidase enzymatic activity by Ca^{2+} ions discovered earlier and indicate that the cation affects intramolecular electron transfer.

DOI: 10.1134/S0006297912080111

Key words: cytochrome *c* oxidase, Ca^{2+} ions, fast kinetics, heme a_3

Cytochrome *c* oxidase (COX) is the terminal enzyme of the respiratory chains of mitochondria and many bacteria, which performs electron transfer to oxygen coupled with membrane potential formation and translocation of H^+ ions through the coupling membrane (see reviews [1-3]). Electron transport is mediated by four redox centers containing transition metal ions. These are two hemes (low-spin heme *a* and high-spin heme a_3) and two copper centers (binuclear (Cu_A) and mononuclear (Cu_B)). Electrons enter the enzyme via Cu_A. Cu_B and the Fe ion of the high-spin heme a_3 are located at a distance of 4.5 Å from each other and form an oxygen-reducing center. The sequence of electron transfer through the enzyme can be described by the scheme:

$$\text{cyt } c \rightarrow Cu_A \rightarrow \text{heme } a \rightarrow \text{heme } a_3/Cu_B \rightarrow O_2.$$

Along with the transient metal ions, mitochondrial COX contains tightly bound Mg^{2+} and Zn^{2+} ions [4] that play structural and, presumably, other functions. Moreover, about 15 years ago the presence of an additional cation-binding site (CBS) in mitochondrial and some bacterial cytochrome oxidases was demonstrated using X-ray structure analysis [5-8], but the role of this site has remained unknown until recently (Fig. 1; see color insert).

The site is located at the very periphery of the main catalytic subunit of the enzyme (subunit I), not far from heme *a* and within just a few angstroms from the enzyme surface protruding from the membrane into the external water phase (Fig. 1a). In the bacterial enzymes, the CBS is occupied by tightly bound calcium ion [6-8]. As for the mitochondrial COX, it was initially presumed that the CBS contained bound Ca^{2+}, but following the data in [9] and taking into account the conditions of crystallization, e.g. the excess of Na^+ in the crystallization buffer, the authors came to conclusion that this is more likely Na^+ ion [5] (Fig. 1b). The structure of the CBS in the animal COX with Ca^{2+} ion bound has not been published yet but has been modeled [10, 11]. It is likely that the doubly charged Ca^{2+} cation interacts in addition to the other groups with the carboxylate of Asp442 next to Ser441, which may form a bond with the cation via a water mole-

Abbreviations: CBS, cation-binding site; COX, cytochrome *c* oxidase; RuAm, hexaammineruthenium ($Ru(NH_3)_6^{3+}$).

* To whom correspondence should be addressed.

cule [10], similarly to the structure resolved for the bacterial enzyme [7, 8].

It is worth noting that reversible selective binding of Ca^{2+} and Na^+ ions, but not of the other metal cations, with cytochrome *c* oxidase was described long before the discovery of the CBS in the 3D-structure of COX. Ca^{2+} was shown to induce a red-shift of the absorption spectrum of heme *a* in mitochondria and in isolated COX [9, 12-14], whereas Na^+ did not affect the spectrum by itself but was able to reverse the Ca-induced spectral shift by displacing Ca^{2+} from the cation-binding site [9, 10, 14]. The equilibrium dissociation constant for Ca^{2+} binding is about 10^{-6} M [9]. One Ca^{2+} ion competes with two Na^+ ions for the cation-binding site, with the affinity of Na^+ ions for the site being three orders of magnitude lower than that of Ca^{2+} [9, 10].

In the bacterial COX, Ca^{2+} ion is tightly bound in the CBS. EGTA is unable to extract the ion, so external Ca^{2+} can not affect spectral properties of the enzyme [9]. It is possible, however, to obtain preparations of bacterial COX by replacing specific amino acid residues [7, 8, 10, 11] that reveal reversible binding of Ca^{2+} and Na^+ similar to that in the mitochondrial enzyme.

The role of the CBS and reversible cation binding in COX has remained obscure for a long time as no influence of calcium or sodium on the enzyme function could be observed. However, in the recent studies of our group, a small Ca-induced shift of the redox midpoint potential, E_m, of heme *a* was observed (about +20 mV) [15, 16], and, in addition, it was found that Ca^{2+} ions inhibit the cytochrome oxidase activity at physiological electron-transfer rates (about 10 sec^{-1}) [17]. In case of the COX from bovine heart muscle, the inhibition was about 50% and was characterized by a titration curve with $K_i \sim 1$ μM that is almost exactly the same as the K_d value determined from the concentration dependence of the Ca-induced red-shift of the heme *a* absorption spectrum obtained for the same sample. Stronger inhibition (up to 80-90%) was observed for COX from liver mitochondria [17]. These results suggest that Ca^{2+} binding in CBS may directly regulate the activity of the mitochondrial cytochrome *c* oxidase, and thus the rate of electron transfer via the entire respiratory chain. This effect may be of great physiological significance, so it is interesting to find out which steps of the catalytic cycle can be affected by the cations.

To reveal the mechanism of the inhibitory action of Ca^{2+} on the COX catalytic activity, we have studied an effect of Ca^{2+} ions on intramolecular electron transfer during reduction of the enzyme by dithionite in the presence of redox-mediator ruthenium(III)hexaammine, $Ru(NH_3)_6^{3+}$ (RuAm). In its reduced form, RuAm is a highly efficient artificial electron donor to COX [18-21], interacting with the enzyme at the same site as cytochrome *c*, the natural donor [19, 21]. It is shown that under these conditions Ca^{2+} induces a retardation of intramolecular electron transfer to hemes *a* and a_3.

MATERIALS AND METHODS

Materials. Sodium dithionite, calcium chloride, and catalase from bovine liver (C-30, 23,000 units/mg protein) were purchased from Sigma-Aldrich (USA), and hexaammineruthenium(III) was from Alfa Division (USA). pH buffers, EGTA, and magnesium sulfate were purchased from Amresco (USA).

The aa_3-type cytochrome *c* oxidase was isolated from bovine heart mitochondria by ammonium sulfate precipitation using a modified protocol by Fowler et al. [22], or from *Rhodobacter sphaeroides* strain containing enzyme with His-tag at subunit I using a Ni^{2+}-affinity column packed with Ni^{2+}-NTA Sepharose from Qiagen (USA) [23]. Dodecyl maltoside of SOL-GRADE purity (Anatrace, USA) was used as a detergent.

Steady-state absorption spectra were recorded with a Cary-300 Bio (Varian, USA) spectrophotometer. Concentration of cytochrome oxidase was determined using molar extinction coefficient $\Delta\varepsilon_{605\text{-}630} = 27\ mM^{-1}\cdot cm^{-1}$ for the "dithionite-reduced *minus* oxidized" difference absorption spectrum.

Fast reduction kinetics was studied with stopped-flow spectrophotometer SX20 (Applied Photophysics, England). The apparatus allows fast recording of absorption spectra in the 350-750 nm range using a photodiode array (up to 1000 spectra per second with programmable distribution of the acquisition points). According to the SX20 manual, mixing time for the 20 μl cuvette with optical path of 10 mm is about 1 msec. Before the start of the experiments, the inner tubing was filled with appropriate buffer without enzyme, and the baseline was recorded.

A typical scheme of the experiment was as follows. Oxidized COX (about 6 μM) in solution containing 100 mM Tris-Hepes buffer with pH 8.0, detergent (0.1% dodecyl maltoside), 100 μM EGTA and, where specified, 200 μM Ca^{2+} or Mg^{2+}, was rapidly mixed with the equal volume of the same buffer with additional 20-40 mM dithionite, necessary concentrations of RuAm, and catalase. The latter was essential for eliminating the traces of hydrogen peroxide, evolving from interaction of dithionite with oxygen. To lower oxygen concentration and prevent hydrogen peroxide formation, the solutions were bubbled with argon for a few minutes before the addition of dithionite. During the mixing dead time and recording of the first spectrum, oxygen in the reaction volume was nearly completely eliminated by its interaction with excess dithionite, and there began reduction of the enzyme. Heme *a* and a_3 reduction was monitored by fast sequential recording of the absorption spectra (400 spectra in time interval from 1 to 10 sec) with an effective photodiode array working range ~350-750 nm. Measurements at shorter wavelengths are limited by the emission spectrum of the xenon lamp. To better resolve the kinetics, we used logarithmic distribution of the sampling points with the maximal resolution in time of 1 msec per spectrum.

To resolve the kinetic components of the spectral changes, three-dimensional arrays obtained in the experiments (absorption/wavelength/time) were examined by the "global analysis" technique implemented in the Pro-Kineticist (Pro-K) program supplied by Applied Photophysics together with the SX20 spectrophotometer. For additional analysis and data presentation, the kinetic curves at selected wavelength were transferred to the Origin 7 program (MicroCal, USA) and were decomposed into exponential components with an aid of the nlreg subroutine (non-linear regression).

RESULTS

Kinetics of heme *a* and a_3 reduction by dithionite in the presence of RuAm. Typical spectral changes observed after fast mixing of the oxidized enzyme with dithionite in the presence of RuAm are shown in Fig. 2.

Figure 2A shows a typical set of absolute absorption spectra recorded after mixing COX with dithionite and RuAm. Direction of the changes with time for different absorption bands is indicated by the arrows. In the Soret region, intensity of the overall absorption band of the oxidized hemes *a* and a_3 at ~420 nm decreases rapidly (absorption maximum of heme a_3^{3+} is located at ~415 nm and that of heme a^{3+} at ~426 nm) while the absorption peak of the reduced hemes at ~444 nm increases. In the visible range, one can observe formation of a peak at ~605 nm, which belongs primarily to the reduced heme *a*. One can notice different behavior of the spectral changes for different bands: in the visible, where heme *a* largely absorbs, the growth of the 605 nm peak is nearly complete after recording of the first several spectra, whereas in the Soret region, where the hemes *a* and a_3 absorb roughly equally, the spectral changes take more time for completion. This suggests that, in agreement with the literature [18, 19], there are fast reduction of heme *a* and much slower reduction of heme a_3 observed in the experiment.

Difference absorption spectra for the same experiment provide a more informative picture of the reaction time-course (Fig. 2B), together with the kinetic curves showing changes of optical density at selected wavelengths (Fig. 2C). The reaction includes at least two phases. In the Soret band, the minimum of difference spectra corresponding to loss of the oxidized heme absorption, shifts rapidly from ~424 nm (characteristic of the oxidized heme *a* decay) to ~415 nm (reflecting progressing decay of the oxidized heme a_3). A set of difference spectra corresponding to the early reaction steps (first 10-20 spectra with an interval between the scans of about 1 msec) is characterized by a nearly isosbestic point at ~432 nm (not shown). This result indicates that redox changes of only one heme take place at this stage. Approximately in the same time range the increase of the maximum at 605 nm (where heme *a* provides the main contribution) is completed (Fig. 2C). Subsequently, the peak at 444 nm and the trough at 415 nm continue to grow for 1-2 sec. At this stage, a new isosbestic point is formed in the Soret region at ~426 nm, characteristic for heme a_3 oxidation-reduction (Fig. 2B).

Global analysis of the data shown in Fig. 2B gives good results for the simplest model including three exponential reaction phases and, correspondingly, four intermediates: a $\rightarrow$ b $\rightarrow$ c $\rightarrow$ d. Analysis according to a two phase model, a $\rightarrow$ b $\rightarrow$ c, yields the spectral line shapes for the intermediates b and c that are nearly identical to those of b and (c + d) in the four intermediate model. However, in this case the agreement of the calculated kinetic curves for $\Delta A_\lambda(t)$ with the experimental curves in the Soret region is much worse. The difference spectra corresponding to the intermediates a, b, c, d and rate constants obtained in this particular experiment are shown in Fig. 2D. To obtain the difference spectra, the first spectrum recorded in 1 msec after mixing was taken as a baseline. Accordingly, the difference spectrum of the initial intermediate, a, is represented in Fig. 2D by the straight line. Intermediate b corresponds to completion of the rapid reaction phase, and intermediates c and d correspond to the two subsequent states generated during the slow phase of spectral changes. One can see that the line shapes of the spectra of intermediates c and d are nearly identical, and both phases b $\rightarrow$ c and c $\rightarrow$ d are characterized by a common isosbestic point at ~426 nm.

Figure 2E shows the difference spectra of the fast and slow phases of COX reduction. The difference spectrum for the first reaction step a $\rightarrow$ b shows a minimum at ~424 nm and two maxima at ~445 and ~605 nm that is typical of heme *a* reduction. It is worth noting that a significant part of this phase occurs during the mixing time, so the magnitude of the spectral changes for the fast component in Fig. 2E is undervalued (and so is the magnitude of the spectrum of intermediate b in Fig. 2D). Moreover, the kinetics of the initial phase is not precisely exponential (see, for example, Fig. 2C). Presumably, the effective mixing takes slightly longer than the value claimed by the manufacturer (1 msec), and this may result in a small lag phase of the response. For these reasons, the rate constant of the first phase, k_1 ~ 200 sec^{-1}, is defined less accurately. Spectral line shapes of the phases b $\rightarrow$ c and c $\rightarrow$ d are practically identical (data not shown). Therefore Fig. 2E gives for simplicity the sum of these two phases, corresponding to the overall slow phase of the reaction b $\rightarrow$ c $\rightarrow$ d. In the Soret region, this slow part is characterized by a difference spectrum that is broader than that of the fast phase, with a maximum at ~443 nm and a minimum at ~412 nm. These characteristics correspond to heme a_3 reduction. In the visible region, the observed changes are very much smaller than for the fast phase. The heme *a* peak at 605 nm is absent, but there is a small α-band maximum at 612 nm and a very broad weak band at 560-580 nm. The low ratio of spectral changes in the α- and γ-

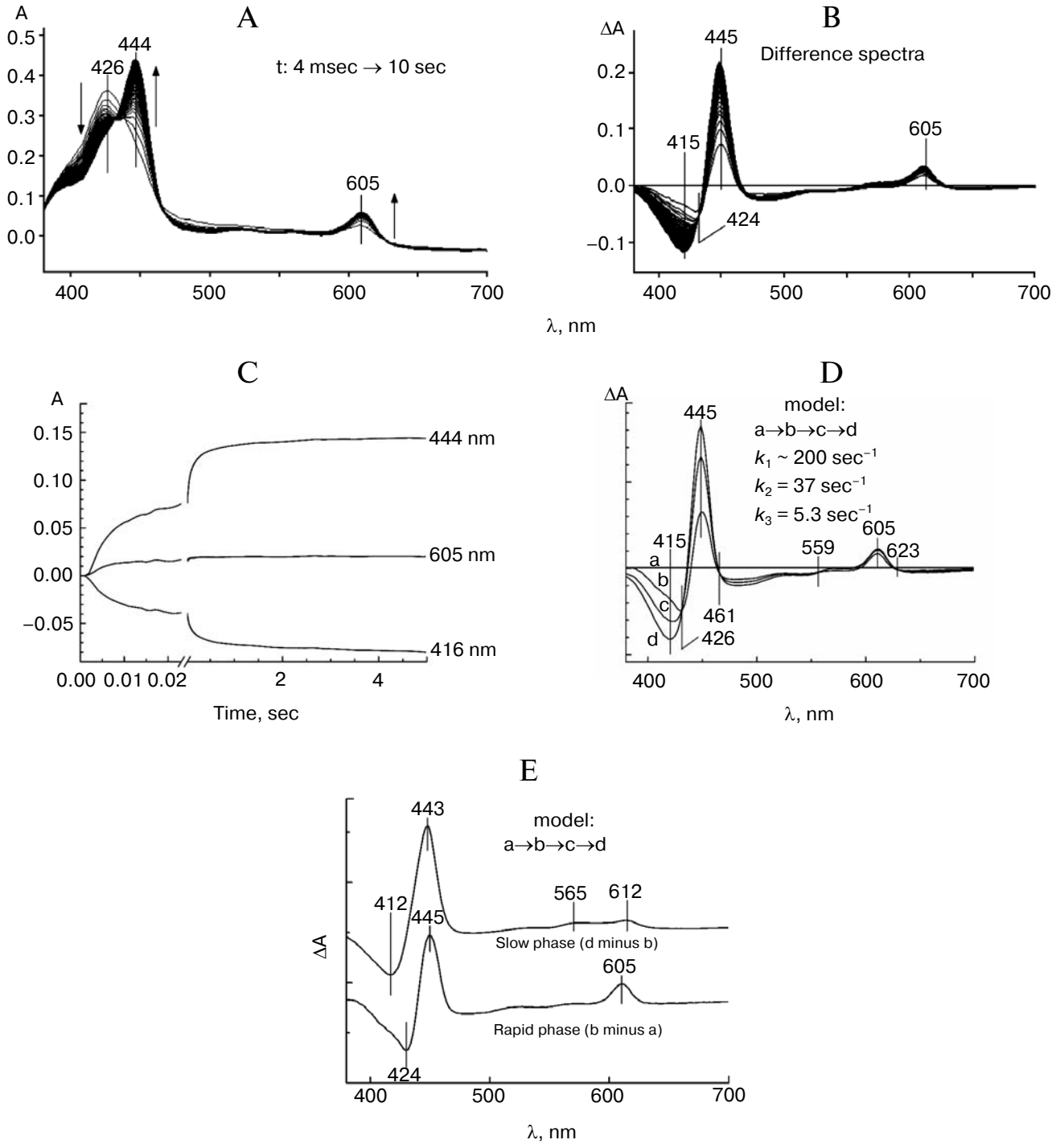

Fig. 2. Kinetics of the spectral changes observed upon COX reduction by dithionite in the presence of RuAm. A) A set of the absolute absorption spectra obtained in a typical experiment. Arrows near the characteristic absorption bands indicate direction of the changes with time. For better visual resolution, only each 10th spectrum is presented. B) Difference spectra for the same experiment; a spectrum, recorded in 1 msec after mixing, is taken as a baseline. C) The kinetics of the absorption changes at some characteristic wavelengths: 416 nm – disappearance of the oxidized forms of hemes *a* and a_3, 445 nm – appearance of the reduced forms of hemes *a* and a_3, 605 nm – mainly formation of the reduced form of heme *a*. D) Resolved spectra of the kinetic intermediates found by standard global analysis of the data on panel (B). E) Line shapes of the difference spectra, characteristic of the rapid and slow phases of the enzyme reduction (correspondingly, reduction of hemes *a* and a_3). Conditions: oxidized COX from beef heart (6 μM) in a buffer containing 100 mM Tris-Hepes, pH 8.0, 0.1% dodecyl maltoside, and 100 μM EGTA was mixed with an equal volume of the same buffer containing additionally 20 mM sodium dithionite, 6 mM ruthenium(III)hexaammine, and catalase to remove H_2O_2 (Sigma, C-30, indicated activity 23,000 units/mg protein, 2 μl/5 ml of the solution). Following the mixing, 400 spectra were scanned during 10 sec with a logarithmic distribution of spectra sampling.

bands ($\alpha/\gamma < 0.1$) is typical of high-spin hemoproteins and verifies that the slow phase corresponds to heme a_3 reduction.

It is noted that the exact values of the rate constants defined by global analysis of the same run can vary (though not that much) depending on the procedure of analysis chosen, for example, with selection of different spectral region or with the length of time domain analyzed. Besides, the approximation of the reaction by a linear sequence of monoexponential phases is, generally speaking, provisional. More precise results can be obtained by preliminary analysis of the entire spectral range followed by optimized global analysis of selected spectral regions and of distinct time intervals. For accurate analysis and for comparison among different experiments, it may be useful sometimes after primary evaluation to transfer the data to the Origin program and perform a standard non-linear regression analysis of the kinetic curves at selected characteristic wavelengths (for example, at 445 nm relative to some reference wavelength). Results of such detailed analysis will be presented elsewhere. In this work, we simply give averaged results for several independent experiments obtained by two different methods, namely, by standard global analysis of spectral changes in the whole range 380-700 nm and by decomposition of kinetics at 445 nm relative to reference wavelength 474 nm into components (see table). Such a comparison gives an idea about the actual accuracy of the calculated absolute rate constants.

The fact really essential for the purposes of this work is that under our experimental conditions, the phases of the fast heme *a* reduction and subsequent intramolecular electron transfer to heme a_3 are well separated. This allows study of the effect of different agents on the rate of intramolecular electron transfer from heme *a* to heme a_3.

Effect of Ca^{2+} ions. The effect of Ca^{2+} on the kinetics of intramolecular electron transfer from heme *a* to heme a_3 has been studied. To this end, experiments analogous to those presented in Fig. 2, have been performed in the presence of 100 μM excess of free Ca^{2+} over EGTA (200 μM Ca^{2+} against 100 μM EGTA). To exclude unspecific effects of Ca^{2+}, control experiments have been carried out with equal concentrations of Mg^{2+} instead of Ca^{2+}, as Mg^{2+} does not interact with the calcium binding site of COX but, similarly to Ca^{2+} ion, binds nonspecifically with the negatively charged sites on the enzyme surface.

Typical kinetic traces of heme a_3 reduction in the presence of Ca^{2+} and Mg^{2+} ions are presented in Fig. 3. One can see that in the presence of Ca^{2+}, electron transfer to heme a_3 in bovine COX is markedly slower than in the presence of Mg^{2+} (Fig. 3a). Mg^{2+} itself does not affect heme a_3 reduction significantly.

The second important control as to the possible unspecific effects of Ca^{2+} is provided by experiments with bacterial COX isolated from *R. sphaeroides*. In the bacterial COX, the CBS is permanently occupied by tightly bound Ca^{2+} ion, which cannot be extracted by EGTA [7]. Accordingly, addition of Ca^{2+} to the wild-type bacterial enzyme does not affect spectral properties of heme *a* or cytochrome *c* oxidase activity of the enzyme [8, 9]. It can be seen that in contrast to the experiments with the mitochondrial enzyme, the traces of heme a_3 reduction in the presence of Ca^{2+} and Mg^{2+} virtually coincide in case of COX from *R. sphaeroides* (Fig. 3b).

The Ca^{2+}-induced inhibitory effect on COX reduction is not that great but is well reproducible (the table), although a minor effect on the rapid first phase of the reaction requires validation. The absolute values of the rate constants obtained for a particular set of data depend somewhat on the specific details of global analysis procedure application (e.g. on a spectral range selected for the analysis and on the length of time span analyzed). With the spectral changes analyzed in the entire wavelength range 380-700 nm within a time interval from 1 msec to 1

Effect of 100 μM Ca^{2+} on the rate constants of heme a_3 reduction

	Rate constant, sec^{-1}			
	global analysis, 380-700 nm range		analysis of the kinetic traces at 445 nm versus the 474 nm reference	
	$+Mg^{2+}$	$+Ca^{2+}$	$+Mg^{2+}$	$+Ca^{2+}$
k_1	190 ± 2	168 ± 8	210 ± 17	176 ± 6.6
k_2	37.3 ± 2	29.7 ± 2.8	30.1 ± 2.1	22.9 ± 1.1
k_3	5.7 ± 0.3	4.3 ± 0.6	5.3 ± 0.14	3.2 ± 0.19

Note: Rate constants are presented for three phases of COX reduction by dithionite in the presence of 3 mM RuAm (mean ± S.E. for six independent experiments with each of the cations). Conditions are described in the legends to Figs. 2 and 3a. For comparison, the results are presented as obtained by two different types of analysis of the data sets: standard global analysis of the overall data file (time span analyzed, 1 msec-1 sec) and decomposition of the kinetic traces at 445 nm versus 474 nm extracted from the overall data file into individual exponentials.

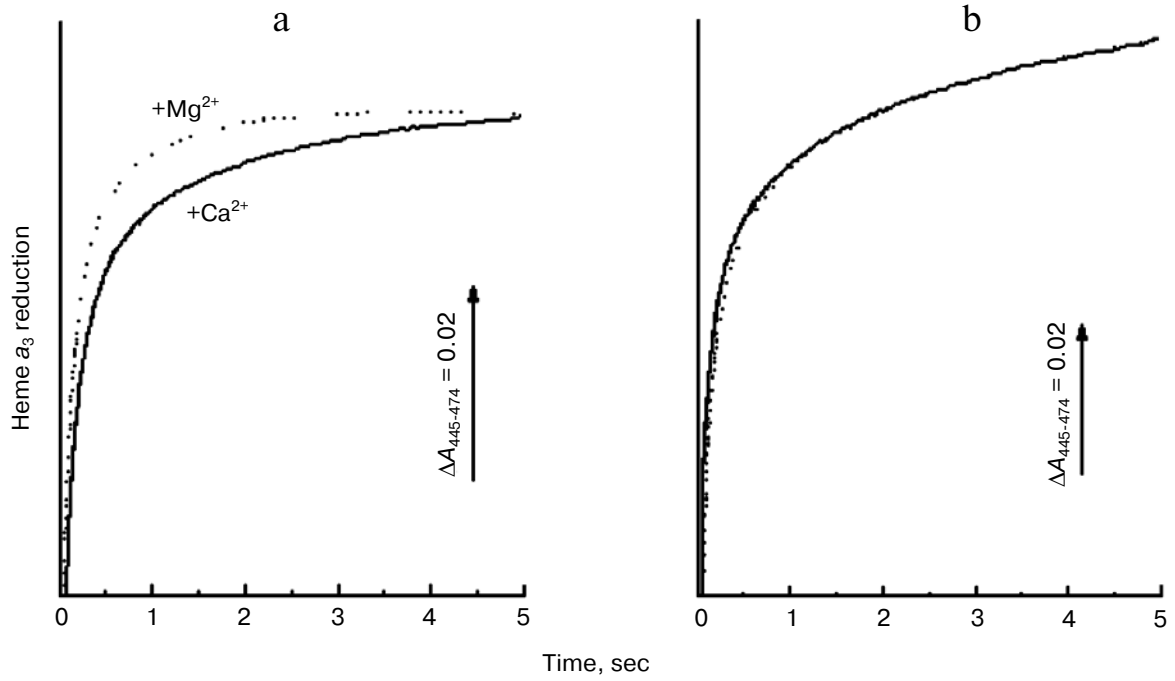

Fig. 3. Deceleration of heme a_3 reduction by Ca^{2+} ions. Conditions as in Fig. 2, but the buffer was supplemented additionally with 100 μM excess of Ca^{2+} or Mg^{2+} ions (200 μM of each cation against 100 μM EGTA). Solid lines, experiment in the presence of Ca^{2+}; dotted line, in the presence of Mg^{2+}. Kinetics of the absorption changes at 445 nm versus the reference at 474 nm was extracted from the overall data file (contributions from reduced hemes *a* and a_3 to A_{445} are roughly equal at this wavelength pair). Only the upper parts of the $\Delta A_{445\text{-}474}$ curves, corresponding to the slow phases of the reaction (heme a_3 reduction), are shown. The rapid initial phase of the curve, dominated by the reduction of heme *a*, is omitted. a) 3 μM bovine COX; b) 2.9 μM bacterial COX from *R. sphaeroides*. In all cases, the concentrations indicated correspond to the final state after mixing.

or 2 sec, the inhibition of heme a_3 reduction rate is 20-30% which is, as discussed below, in reasonable agreement with the inhibition of the steady-state cytochrome *c* oxidase activity of bovine COX by ~50% [17]. The inhibition increases to 30-50% and even more if we include in the analysis the data on a longer time scale (5-10 sec), however such an analysis seems to be less reliable because of interference of the slow absorption drifts beyond the reaction timescale increases.

DISCUSSION

COX reduction by dithionite in the presence of RuAm at high concentrations. To evaluate the site of the Ca^{2+} effect on the intramolecular electron transport in COX, pre-steady state kinetics of reduction of the oxidized COX by dithionite has been studied under anaerobic conditions in the presence of redox-mediator $[Ru(III)(NH_3)_6]^{3+}$ (RuAm) at high concentrations. $Na_2S_2O_4$ is thermodynamically a very strong reductant (effective redox potential of a millimolar dithionite solution is about −0.6 V). However, in the reaction of COX reduction [24, 25], dithionite is not that active kinetically for several reasons. First, steady-state concentration of the active species, anion-radical $SO_2^{\cdot-}$, formed by fast equilibrium dissociation of dithionite dianion ($S_2O_4^{2-} \leftrightarrow 2\ SO_2^{\cdot-}$, $K = 1.4 \cdot 10^{-9}$ M [26]), is within the micromolar range at the commonly used dithionite concentrations of ~10^{-2} M. Second, the site of electron entry in COX, Cu_A, is surrounded by negatively charged carboxylic groups that stimulates interaction of the enzyme with the positively charged natural electron donor cytochrome *c* but impedes reaction with negatively charged reductants including anion-radical $SO_2^{\cdot-}$. The $[Ru(III)(NH_3)_6]^{3+}$ cation is reduced to $[Ru(II)(NH_3)_6]^{2+}$ by excess of negatively charged dithionite, and at concentrations of ~10^{-3} M it delivers electrons to Cu_A in COX much faster than dithionite itself. It was shown that within the range studied 40-200 μM, the rate of reaction depends linearly on RuAm concentration with $k_v \sim 5 \cdot 10^5$ $M^{-1} \cdot sec^{-1}$ at pH 6.0 [18]. Actually, the role of dithionite under these conditions is to remove oxygen and to maintain RuAm in a fully reduced state. Varying concentrations of added RuAm, it is possible to modify over a wide range the rate of electron input into the enzyme from the excess dithionite. The sequence of electron transfer under these conditions can be described by the simplified scheme:

dithionite → RuAm → Cu_A → heme *a* → heme a_3/Cu_B,

where the reduced RuAm serves as the actual electron donor. Reduction of heme *a* and a_3 is easily followed spectrophotometrically, while Cu ions contribute but little to absorption changes as compared to the hemes. Intramolecular electron transfer from Cu_A to heme *a* is very fast ($\tau \sim 50$ μsec [27, 28]). Therefore, the rapid mixing technique with millisecond time resolution allows following the reduction of heme *a*, the rate of which is determined by the rate of electron input from Ru(II)Am to Cu_A, and the subsequent intramolecular electron transfer from heme *a* to heme a_3 in the oxygen-reduction center of the enzyme [18, 20]. Spectral changes of hemes *a* and a_3 strongly overlap in the Soret region, so it is necessary to find conditions under which redox transitions of the two hemes are separated in time.

To obtain the rates of heme *a* and a_3 reduction in different forms of the oxidized COX, Palmer's laboratory employed an experimental technique based on the use of excess dithionite in the presence of millimolar concentrations of RuAm [29, 30]. Under these conditions, heme *a* reduction occurs partly during the time of mixing already and is well separated kinetically from the subsequent intramolecular electron transfer from heme *a* to heme a_3, the rate of which is independent of RuAm concentration [18, 20]. Such an experimental model allows study of the effects of various agents on the intramolecular electron transfer from heme *a* to heme a_3, and we used this approach in this work to evaluate the effect of Ca^{2+} ions on the rate of heme a_3 reduction.

We were able to reproduce the conditions under which the relatively slow reduction of heme a_3 is well separated in time from the fast reduction of heme *a*. The results are generally in agreement with the literature [19, 20, 29, 30]. As in the experiments described in [29, 30], we observed three phases of reaction: rapid, only partly resolved reduction of heme *a* ($k_1 \sim 200$ sec^{-1}), and two phases of heme a_3 reduction with rate constants differing from each other by an order of magnitude (k_2 = 30-40 sec^{-1}, k_3 = 5-6 sec^{-1}). The absolute values of the rate constants of heme a_3 reduction in our experiments are slightly lower (~1.5-fold) than in [29, 30]. These discrepancies could be explained by different properties of COX preparations (characteristics of the oxidized COX are known to vary considerably for different preparations [31]), as well as by more alkaline pH values of the media and some other differences in the experimental conditions. It is also noted that at pH > 7.0, there is increased probability of RuAm alkaline hydrolysis [18] so that the actual concentration of RuAm in our experiments might be lower than in references [29, 30], which may explain in part slower reduction of heme *a*, the rate of which is proportional to concentration of RuAm [18].

Reasons for the biphasic reduction of heme a_3. Reduction of heme a_3 has a pronounced biphasic character in agreement with the data of Palmer's group obtained under similar conditions [29, 30]. In our experiments, contribution of the slowest phase with $k_3 \sim 5$ sec^{-1} is significantly less than the contribution of the middle phase with $k_2 \sim 40$ sec^{-1}. Such ratio of contributions is typical of the so-called "fast" (activated) COX preparations [29] and correlates with the position of the Soret band at ~426 nm in the oxidized enzyme. In the "slow" preparations of the enzyme, the Soret peak of the oxidized form is shifted to 417-420 nm [31], and contributions of the two phases of heme a_3 reduction are roughly equal [29]. The first obvious reason for the biphasic character of electron transfer to heme a_3 might consist in the well-known heterogeneity of heme a_3 state in the oxidized enzyme [2, 31]. Second, the reduction of the oxygen-reducing center, a_3/Cu_B, involves in fact two competing processes. In a fraction of the enzyme population, the first electron delivered to this center from heme *a* is transferred to heme a_3, so that heme a_3 is reduced under the conditions when Cu_B is oxidized. In the other fraction of the enzyme molecules, the first electron is transferred from heme *a* to Cu_B, and only the second electron goes to heme a_3, so that heme a_3 undergoes reduction under the conditions when Cu_B is already reduced [30]. Taking into account anticooperative redox interactions between heme a_3 and Cu_B [1-3], the two pathways of heme a_3 reduction are expected to be characterized by significantly different values of the rate constants; namely, reduction of Cu_B by the first electron should slow down reduction of heme a_3 by the second electron.

Revealing the difference spectrum of heme a_3 in the visible region. Absorption spectra of the two *a*-type hemes in COX are strongly overlapping [32]. In the Soret band, hemes *a* and a_3 have similar contribution to the absorption, and individual spectra of hemes *a* and a_3 have been resolved quite a long time ago. At the same time, the absorption of COX in the α-band is dominated ~90% by the low-spin heme *a* both in the oxidized and reduced forms of COX. Therefore, it is difficult to reveal experimentally characteristics of the absorption spectrum of heme a_3 in the visible against the background of the dominating contribution of heme *a*, and, accordingly, the line shape of heme a_3 α-band in the aa_3-type oxidases has remained unknown. According to the indirect calculations, based on comparison of the static absorption spectra of mitochondrial COX in the presence of different ligands, the difference spectrum of heme a_3 (reduced *minus* oxidized) is characterized in the visible region by a weak α-band with a maximum at ~603 nm and a narrow β-band at ~565 nm [32]. At the same time, experiments with the ba_3-type COX from the thermophilic bacterium *Thermus thermophilus* in which the absorption bands of the low-spin heme *b* and the high-spin heme a_3 in the visible are well separated, show that the reduced heme a_3 in this enzyme is characterized by a maximum of the α-band at 613 nm [33, 34].

It is therefore interesting to note that the spectrum of the slow phase of absorption changes that is observed dur-

ing COX reduction by dithionite in the presence of RuAm and which corresponds in all probability to the reduction of heme a_3, is characterized by a weak peak at 612 nm with $\Delta\varepsilon_{612\text{-}630} \sim 5\ mM^{-1}\cdot cm^{-1}$ (Fig. 2D), which is similar to characteristics of heme a_3 in ba_3 oxidase. The data, however, may not be sufficient for final conclusions because it cannot be excluded that heme a_3 and/or Cu_B reduction is accompanied by a small change in a line shape of the intensive absorption band of the reduced heme *a*, which overlaps the difference spectrum of heme a_3. Additional experiments are necessary. Unfortunately, in the preceding papers of Palmer's group [29, 30] only the kinetics of the absorption changes at selected wavelengths was presented with no spectra of the individual phases of COX reduction by dithionite + RuAm; therefore, it is not possible to compare our results with the data obtained by those authors in this respect.

Effect of calcium ions. The principal result of this work consists in revealing the effect of Ca^{2+} on the rate of intramolecular electron transfer in COX. The observed effect is modest, 20-30%, which however, is comparable to the roughly 2-fold decrease in the cytochrome *c* oxidase activity induced by Ca^{2+} ions as revealed in our previous studies [16, 17]. Control experiments with addition of Mg^{2+} instead of Ca^{2+} indicate that the effect is specific for calcium ions. Also, the absence of the calcium-induced effect in case of the bacterial COX in which the specific cation-binding site is pre-occupied by tightly bound Ca^{2+} ion confirms the specificity of the calcium effect.

Deceleration of electron transport from heme *a* to heme a_3 may be a consequence of a small (15-20 mV) increase of heme *a* midpoint redox potential, E_m, induced by Ca^{2+} ions [15]. Such a shift of E_m corresponds to roughly a 2-fold change in redox equilibrium constant, K_{eq} between heme *a* and heme a_3. K_{eq} is related to the rate constants of electron transfer from heme *a* to heme a_3 (k_1) and the reversed reaction (k_{-1}) by the ratio $K_{eq} = k_1/k_{-1}$. Accordingly, decrease of K_{eq} must be accompanied by a decrease of rate constant, k_1, of electron transfer from heme *a* to heme a_3 and/or by an increase in the rate constant of the reversed reaction, k_{-1}. In a typical case, when a change in K_{eq} value is bound to simultaneous decrease of k_1 and increase of k_{-1} by the same percentage, the twofold change in K_{eq} would be accompanied by a decrease of k_1 ~1.4-fold, i.e. by ~30%, that is in good agreement with our data.

More detailed analysis of the kinetics of heme a_3 reduction in our experimental system and relation of the observed effective rate constant of heme a_3 reduction with the true microscopic rate constants of electron transport between all the redox centers of enzyme is beyond the scope of this work and will be considered elsewhere together with a more detailed set of data.

To clarify the mechanism of Ca^{2+} inhibitory action, it would be worthwhile to study the effect of the cation on the kinetics of heme a_3 reduction in liver COX, where the Ca^{2+}-induced inhibition of activity is much stronger than in COX from heart.

This work was supported by a grant of the Russian Foundation for Basic Research (No. 11-04-01330-a) and by an International Research Scholar Award 55005615 from the Howard Hughes Medical Institute.

REFERENCES

1. Ferguson-Miller, S., and Babcock, G. T. (1996) *Chem. Rev.*, **7**, 2889-2907.
2. Belevich, I., and Verkhovsky, M. I. (2008) *Antiox. Redox Signal.*, **10**, 1-29.
3. Yoshikawa, S., Muramoto, K., and Shinzawa-Itoh, K. (2011) *Annu. Rev. Biophys.*, **40**, 205-223.
4. Tsukihara, T., Aoyama, H., Yamashita, E., Takashi, T., Yamaguichi, H., Shinzawa-Itoh, K., Nakashima, R., Yaono, R., and Yoshikawa, S. (1996) *Science*, **272**, 1136-1144.
5. Yoshikawa, S., Shinzawa-Itoh, K., Nakashima, R., Yaono, R., Inoue, N., Yao, M., Fei, M. J., Libeu, C. P., Mizushima, T., Yamaguchi, H., Tomizaki, T., and Tsukihara, T. (1998) *Science*, **280**, 1723-1729.
6. Ostermeier, C., Harrenga, A., Ermler, U., and Michel, H. (1997) *Proc. Natl. Acad. Sci. USA*, **94**, 10547-10553.
7. Pfitzner, U., Kirichenko, A., Konstantinov, A. A., Mertens, M., Wittershagen, A., Kolbesen, B. O., Steffens, G. C. M., Harrenga, A., Michel, H., and Ludwig, B. (1999) *FEBS Lett.*, **456**, 365-369.
8. Lee, A., Kirichenko, A., Vygodina, T., Siletsky, S. A., Das, T. K., Rousseau, D. L., Gennis, R. A., and Konstantinov, A. A. (2002) *Biochemistry*, **41**, 8886-8898.
9. Kirichenko, A., Vygodina, T. V., Mkrtchyan, H. M., and Konstantinov, A. A. (1998) *FEBS Lett.*, **423**, 329-333.
10. Kirichenko, A. V., Pfitzner, U., Ludwig, B., Soares, C. M., Vygodina, T. V., and Konstantinov, A. A. (2005) *Biochemistry*, **44**, 12391-12401.
11. Riistama, S., Laakkonen, L., Wikstrom, M., Verkhovsky, M. I., and Puustinen, A. (1999) *Biochemistry*, **38**, 10670-10677.
12. Wikstrom, M., and Saari, H. (1975) *Biochim. Biophys. Acta*, **408**, 170-179.
13. Saari, H., Pentilla, T., and Wikstrom, M. (1980) *J. Bioenerg. Biomembr.*, **12**, 325-338.
14. Mkrtchyan, H., Vygodina, T., and Konstantinov, A. A. (1990) *Biochem. Int.*, **20**, 183-190.
15. Vygodina, T. V., Ptushenko, V. V., and Konstantinov, A. A. (2008) *Biochim. Biophys. Acta*, **1777**, S110-S111.
16. Konstantinov, A. A. (2010) *Biochim. Biophys. Acta*, **1797** (Suppl.), 92.
17. Vygodina, T. V., and Konstantinov, A. A. (2010) *Biochim. Biophys. Acta*, **1797**, 102.
18. Scott, R. A., and Gray, H. B. (1980) *J. Am. Chem. Soc.*, **102**, 3219-3224.
19. Hochman, J. H., Partridge, B., and Ferguson-Miller, S. (1981) *J. Biol. Chem.*, **256**, 8693-8698.
20. Reichardt, J. K. V., and Gibson, Q. H. (1982) *J. Biol. Chem.*, **257**, 9268-9270.

21. Tsofina, L. M., Liberman, E. A., Vygodina, T. V., and Konstantinov, A. A. (1986) *Biochem. Int.*, **12**, 103-110.
22. Fowler, L. R., Richardson, S. H., and Hatefi, Y. (1962) *Biochim. Biophys. Acta*, **64**, 170-173.
23. Mitchell, D. M., and Gennis, R. B. (1995) *FEBS Lett.*, **368**, 148-150.
24. Halaka, F. G., Babcock, G. T., and Dye, J. L. (1981) *J. Biol. Chem.*, **256**, 1084-1087.
25. Orii, Y. (2008) *J. Bioenerg. Biomembr.*, **30**, 47-53.
26. Lambeth, D. O., Campbell, K. L., Zand, R., and Palmer, G. (1973) *J. Biol. Chem.*, **248**, 8130-8136.
27. Nilsson, T. (1992) *Proc. Natl. Acad. Sci. USA*, **89**, 6497-6501.
28. Zaslavsky, D., Kaulen, A., Smirnova, I. A., Vygodina, T. V., and Konstantinov, A. A. (1993) *FEBS Lett.*, **336**, 389-393.
29. Jancura, D., Antalik, M., Berka, V., Palmer, G., and Fabian, M. (2006) *J. Biol. Chem.*, **281**, 20003-20010.
30. Jancura, D., Berka, V., Antalik, M., Bagelova, J., Gennis, R. B., Palmer, G., and Fabian, M. (2006) *J. Biol. Chem.*, **281**, 30319-30325.
31. Moody, A. J. (1996) *Biochim. Biophys. Acta*, **1276**, 6-20.
32. Wikstrom, M., Krab, K., and Saraste, M. (1981) *Cytochrome Oxidase – a Synthesis*, Academic Press, N. Y.
33. Zimmermann, B. H., Nitsche, C. I., Fee, J. A., Rusnak, F., and Munck, E. (1988) *Proc. Natl. Acad. Sci. USA*, **85**, 5779-5783.
34. Oertling, W. A., Surerus, K. K., Einarsdottir, O., Fee, J. A., Dyer, R. B., and Woodruff, W. H. (1994) *Biochemistry*, **33**, 3128-3141.